

## Wavelet Video Coding Algorithm Based on Energy Weighted Significance Probability Balancing Tree

Chuan-Ming Song<sup>1,2,3</sup> · Bo Fu<sup>1</sup> ·  
Xiang-Hai Wang<sup>1,\*</sup> · Ming-Zhe Fu<sup>1</sup>

Received: date / Accepted: date

**Abstract** This work presents a 3-D wavelet video coding algorithm. By analyzing the contribution of each biorthogonal wavelet basis to reconstructed signal's energy, we weight each wavelet subband according to its basis energy. Based on distribution of weighted coefficients, we further discuss a 3-D wavelet tree structure named **significance probability balancing tree**, which places the coefficients with similar probabilities of being significant on the same layer. It is implemented by using hybrid spatial orientation tree and temporal-domain block tree. Subsequently, a novel 3-D wavelet video coding algorithm is proposed based on the energy-weighted significance probability balancing tree. Experimental results illustrate that our algorithm always achieves good reconstruction quality for different classes of video sequences. Compared with asymmetric 3-D orientation tree, the average peak signal-to-noise ratio (PSNR) gain of our algorithm are 1.24dB, 2.54dB and 2.57dB for luminance (Y) and chrominance (U,V) components, respectively. Compared with temporal-spatial orientation tree algorithm, our algorithm gains 0.38dB, 2.92dB and 2.39dB higher PSNR separately for Y, U, and V components. In addition, the proposed algorithm requires lower computation cost than those of the above two algorithms.

**Keywords** Video coding · scalable coding · 3-D wavelet transform · weighted tree · significant coefficient

---

\*Corresponding author: Xiang-Hai Wang  
E-mail: chmsong@163.com  
Tel.: +86-411-85827711

<sup>1</sup> School of Computer and Information Technology, Liaoning Normal University, Dalian 116029, China

<sup>2</sup> School of Computer Science and Technology, Dalian University of Technology, Dalian 116024, China

<sup>3</sup> State Key Laboratory for Novel Software Technology, Nanjing University, Nanjing 210093, China

## 1 Introduction

As the rapid development of Internet, wireless communication, and pervasive computing, many multimedia services has been provided in various applications [1], such as video telephony/conferencing, mobile streaming [2], wireless LAN video, broadband video distribution, professional video manipulation [3], visual surveillance [4,5,6], visual retrieval [7,8], visual recognition [9], visual analysis [10,11,12,13], and etc. These applications are able to realize cross-platform and real-time communication for clients with different power, display resolution, and bandwidth. In these scenarios, progressive video transmission and multi-quality services are required due to various user requirements, client capabilities, and transmission conditions (e.g., noise and congestion) over heterogeneous networks. This issues a great challenge to state-of-the-art video coding techniques, and has attracted intensive attentions over the past decade. Scalable video coding (SVC) is one of the effective solutions to this problem [14], which encodes a video sequence once and decodes it many times in different versions so as to efficiently adapt to the application requirements.

All the existing scalable video coding approaches can be divided into two categories. The first category represented by MPEG-x or H.26x standards is based on closed-loop hybrid prediction and discrete cosine transform (DCT) structure, such as SVC amendment of H.264/MPEG-4 AVC [15,16,17] and scalable extension of HEVC [18,19,20,21]. The second category employs wavelet-based closed-loop [22,23,24] or open-loop prediction structure [25,26,27]. The multi-resolution property intrinsically enables wavelet transform to implement scalable video coding more easily and flexibly than DCT. In addition, wavelet transform presents superior nonlinear approximation performance to DCT, contributing to coding efficiency improvement. Thus, when MPEG (Moving Picture Expert Group) called for proposals for SVC in 2003, 14 schemes were totally received worldwide, 12 of which addressed the scalable video coding using wavelet-based approach. Moreover, studies show that closed-loop prediction structure is more efficient than open-loop one only when the target bitrate is known, while the latter structure tends to gain superior or approximately equivalent performance to the former in other conditions [28]. Therefore, 3-D wavelet-based scalable video coding (WSVC) exhibits great potentials and has been widely appreciated. So far, many WSVC approaches have been proposed such as 3-D SPIHT [25], MC-EZBC [26], VidWav platform [27], and [29,30,31,32,33,34,35]. And the Joint Video Team (JVT) originated an ad-hoc group on “further exploration on wavelet video coding” in October 2004 to enhance its coding efficiency [36]. Besides all the features, e.g. spatial and temporal scalability, provided by state-of-the-art scalable coding approaches, wavelet video coding will realize more promising functionalities [37] such as very high number of spatio-temporal decomposition levels, nondyadic spatial resolution, extremely fine grain SNR scalability, and better rate-distortion performance for very high resolution material. So far, comparison studies have demonstrated that the WSVC provides better coding performance than those of SVC amendment of H.264/MPEG-4 AVC and the Motion JPEG-2000 [38]. And the

performance of the SVC amendment and Motion JPEG2000 depends on the resolution of coded video sequences. However, the coding efficiency of state-of-art wavelet video coding is still slightly inferior to that of HEVC/H.265 standard. It is thus much necessary to investigate wavelet-based video coding and further improve its rate-distortion performance.

This study presents a 3-D wavelet video coding algorithm based on energy-weighted significance probability balancing tree. The basic idea is to weight each subband according to its wavelet basis' energy. Subsequently, the weighted coefficients are encoded using an asymmetric tree that places the coefficients with similar probabilities of being significant on the same layer. Our algorithm enjoys the following advantages not shared by conventional methods.

- By exploiting the energy distribution of wavelet bases over different subbands, the energy-based weight can facilitate in theory better rate-distortion performance, as well as smaller mean squared error (MSE). Moreover, the subband weight raises the zerotree ratio, decreasing the synchronization information cost.
- The significance probability balancing tree puts those coefficients with similar probabilities of being significant on the same layer. Hence, the coefficients which has small probability of being significant will be moved toward leaf nodes. Through this way, we are able to obtain as many zerotrees as possible, and to place significant coefficients at the front of bitstream.
- Taking into account intra-scale relationship between neighboring coefficients, the synchronization bits are encoded block by block instead of the coefficient by coefficient manner of conventional algorithms. Both the synchronization information and computational complexity are thus efficiently reduced.

The remainder of this paper is organized as follows. Section II overviews related works. Section III discusses the biorthogonal wavelet bases' energy of different subbands, as well as the weight of each subband. Section IV presents a novel 3-D wavelet tree structure based on subband weight. The proposed algorithm is detailed in Section V. We evaluate our algorithm in Section VI and conclude the whole paper in the last section.

## 2 Related Works

Wavelet-based image and video coding has to address two key issues, namely to encode the magnitude and location of each significant coefficient using as less bits as possible called “synchronization information”. For the first aspect, most algorithms employ successive approximation quantization based on bitplane to encode significant coefficients' magnitudes, while EBCOT algorithm uses a fractional bitplane technique [39]. These algorithms believe that the bits on the same bitplane have equal importance for the reconstructed image or video quality regardless of whether they are in the same subband or not. In fact, this study will illustrate that the energies of biorthogonal wavelet bases spanning

different subbands generally vary. Thus, one bit cannot obtain identical energy with that on the same bitplane but in a different subband. This indicates bitplane coding will not achieve optimal rate-distortion performance. For the second aspect, EZW [40], SPIHT [41], and SLCCA [42] employ zerotree to locate significant coefficients according to magnitude attenuation from coarse to fine scales. In contrast, SPECK [43], EZBC [44], and EBCOT use block, called zeroblock, as a unit to transmit synchronization information exploiting intra-scale correlation of wavelet coefficients.

Moinuddin *et al.* pointed out that the tree structure plays a significant role in improving 3-D wavelet video coding efficiency [45,46]. Motivated by the zerotree and zeroblock in image compression, researchers extended symmetrically these two 2-D structures to 3-D cases for video coding [25,26,47,48,49,50,51,52,53], e.g. [47], [48], [25] and [49], [50], and [26] are separately the extensions of EZW, SLCCA, SPIHT, EBCOT, and EZBC. Nevertheless, the wavelet coefficient distribution of still images is obviously different from that of video frames, especially temporal high-pass frames. [54] calculates the average standard deviation (STD) of Carphone, Mother & Daughter, and Hall Monitor sequences along horizontal, vertical, and temporal direction. Statistics show that the STD along temporal direction is much smaller than the STDs along the other two directions, while the STDs along horizontal and vertical direction are very close. In this case, the amplitudes of temporal high-pass coefficients tend to be smaller than those of spatial high-pass coefficients. The probabilities of the coefficients on the same layer being significant are nonuniform under such a symmetric tree structure. As a result, part of the synchronization information is wasted, inevitably affecting the overall coding efficiency. In general, instead of intuitively extending zerotree or zeroblock from 2-D to 3-D case, the distribution characteristics of wavelet coefficients should be taken into account when designing tree structure. This will definitely reduce further the overhead of synchronization information and achieve better rate-distortion performance.

Kim *et al.* use an approximate symmetry tree structure in [25] and obtain superior coding efficiency to symmetry tree structure. However, the approximate symmetry tree requires that the numbers of wavelet decomposition along spatial and temporal directions be equal. This restriction cannot fully exploit the redundancy along temporal direction. To address this issue, an asymmetric 3-D orientation tree is proposed in [54] which attaches all subbands together to form a longer subband tree. This asymmetric 3-D orientation tree has no limitation on the number of wavelet decomposition along each direction and outperforms 3-D SPIHT. Compared with symmetric tree structure, the asymmetric structure in [54] is capable of gathering more insignificant coefficients, requiring less synchronization bits. In order to build a longer tree, a virtual zerotree [29,55] is proposed as an extension of existing tree structures. It virtually creates zerotrees in  $LL$  subband so that the significant map can be coded in a more efficient way, although no decimation and decomposition actually takes place. However, [29,54,55] is still ignored the nonuniform probabilities of spatio-temporal coefficients being significant on the same layer. Considering

this fact, Zhang *et al.* [56] decomposes a spatio-temporal orientation tree into a temporal direction tree and a spatial orientation tree. Moreover, the temporal direction trees are encoded with a higher priority over spatial orientation trees. Only when a temporal direction tree has a significant coefficient, the spatial orientation tree which the significant temporal coefficient belongs to will be scanned. This method however may delay the coding of isolated zeros in spatial orientation trees.

We have discussed the inter-scale correlation of wavelet coefficients above. In fact there is another correlation, i.e. intra-scale correlation. For the video sequence following a stable random process, the intra-scale correlation is even stronger than inter-scale correlation [57]. On the basis of asymmetric spatio-temporal orientation tree, [45,58] introduce the zeroblock structure of size  $2 \times 2$  pixels into 3-D video coding and code the synchronization information using zeroblock as a unit. Since this method takes advantage of correlations of both inter- and intra-scale, its video coding efficiency is effectively improved. But [45,58] treat the coefficients in different subbands indiscriminately. In the next section, we will discuss the unequal roles of different subbands in terms of energy for the reconstructed image/video quality.

### 3 Energy-Based Weight of Wavelet Coefficients

Most state-of-the-art wavelet-based video coders employ biorthogonal wavelet transform and encode significant coefficients bitplane by bitplane. These approaches believe the bits on the same bitplane in different subbands are of equal importance. However, [59,60] points out that biorthogonal wavelet transform does not have energy-preserving property. Consequently, the coefficients in separate subbands work differently for the reconstructed signal energy.

Let  $g$  and  $h$  be the low-pass and high-pass filter of biorthogonal wavelet, whose length are  $M$  and  $N$ , respectively. Their dual filters are separately  $\tilde{g}$  and  $\tilde{h}$ . And the low-frequency and high-frequency coefficients under scale  $j$  are denoted by  $a_i^j$  and  $b_i^j$ , in which  $0 \leq i < L$  and  $L$  is the length of low-frequency and high-frequency components. Then the 1-level inverse wavelet transform can be expressed as follows,

$$a^{j+1} = \tilde{g} * (Ua^j) + \tilde{h} * (Ub^j), \quad (1)$$

where  $U$  and “\*” are up-sampling and convolution operators, respectively. Because wavelet transform  $f$  is linear, we have  $f(x) = xf(1)$ . Thus we only need to examine the energy of unit coefficient in each subband to prove that the bases of separate subbands contribute differently to reconstructed image/video.

**Theorem 1 (Wavelet bases’ energy)** *Let  $a_K^j = 1$  ( $K$  is a constant,  $\lfloor N/2 \rfloor \leq K \leq L - \lfloor N/2 \rfloor$ ), while the other coefficients in  $a^j$  and all coefficients in  $b^j$  be 0. Suppose the reconstructed energy after inverse transform is  $E_a$ . Likewise, set  $b_K^j = 1$  ( $K$  is a constant,  $\lfloor M/2 \rfloor \leq K \leq L - \lfloor M/2 \rfloor$ ), while the other*

**Table 1** Weights of Spatio-temporal Subbands After a 4-level Temporal Decomposition Followed by a 3-level Spatial Decomposition

	$LL_3$	$LH_3$	$HL_3$	$HH_3$	$LH_2$	$HL_2$	$HH_2$	$LH_1$	$HL_1$	$HH_1$
$LLLL$	9.71	7.31	7.31	5.50	5.28	5.28	3.87	4.04	4.04	3.15
$LLLH$	4.03	3.04	3.04	2.28	2.19	2.19	1.61	1.68	1.68	1.31
$LLH_1$	2.98	2.24	2.24	1.69	1.62	1.62	1.19	1.24	1.24	0.97
$LLH_2$	3.98	2.99	2.99	2.25	2.16	2.16	1.58	1.66	1.66	1.29
$LH_1$	2.17	1.63	1.63	1.22	1.18	1.18	0.87	0.90	0.90	0.70
$LH_2$	2.33	1.75	1.75	1.32	1.27	1.27	0.93	0.97	0.97	0.75
$LH_3$	2.49	1.88	1.88	1.41	1.36	1.36	0.99	1.04	1.04	0.81
$LH_4$	2.77	2.09	2.09	1.57	1.51	1.51	1.10	1.15	1.15	0.90
$H_1$	2.06	1.55	1.55	1.17	1.12	1.12	0.82	0.86	0.86	0.67
$H_2$	2.06	1.55	1.55	1.17	1.12	1.12	0.82	0.86	0.86	0.67
$H_3$	2.06	1.55	1.55	1.17	1.12	1.12	0.82	0.86	0.86	0.67
$H_4$	2.06	1.55	1.55	1.17	1.12	1.12	0.82	0.86	0.86	0.67
$H_5$	2.06	1.55	1.55	1.17	1.12	1.12	0.82	0.86	0.86	0.67
$H_6$	2.06	1.55	1.55	1.17	1.12	1.12	0.82	0.86	0.86	0.67
$H_7$	2.13	1.60	1.60	1.20	1.15	1.15	0.85	0.85	0.88	0.67
$H_8$	1.94	1.46	1.46	1.10	1.06	1.06	0.77	0.81	0.81	0.67

coefficients in  $b^j$  and all coefficients in  $a^j$  to be 0. Let the energy after inverse transform now be  $E_b$ . Then we have  $E_a \neq E_b$ .

**Proof:** In the case of  $a^{j+1} = \tilde{g} * (Ua^j)$ , from the procedure of wavelet transform, a nonzero value will produce only if the filter coefficients coincide with  $a_K^j$ . Then we have  $E_a = \sum_{l=0}^{N-1} (\tilde{g}_l)^2$ , where  $\tilde{g}_l$  stands for the  $l$ th filter coefficient of  $\tilde{g}$ . Similarly, we can obtain  $E_b = \sum_{l=0}^{M-1} (\tilde{h}_l)^2$  in the case of  $a^{j+1} = \tilde{h} * (Ub^j)$ . For all commonly used biorthogonal wavelets in image and video compression, e.g. Daubechies 9/7 and 5/3 wavelet, their sums of squared filter coefficients are not equal. Therefore, we conclude that  $E_a \neq E_b$ .

Theorem 1 indicates that we cannot achieve the minimized MSE if we employ traditional bitplane technique to encode all subbands' coefficients. We thus propose to weight the wavelet coefficients subband by subband before bitplane coding. The weight of each subband equals the square root of its unit coefficient's energy. Note that the subband weight varies with its corresponding wavelet basis. Table 1 lists the weights of 160 temporal-spatio subbands obtained by a 4-level 5/3 temporal decomposition followed by a 3-level 9/7 spatial decomposition, in which the line and column represent temporal and spatial subbands, respectively. From Table 1 we can find that the lower the subband, the larger the weight. Moreover, there exist obvious differences among the weights of different subbands. This result not only verifies Theorem 1, but also illustrates the necessity of weighting wavelet coefficients.

**Table 2** Average Energy Comparison Between Spatial and Temporal High-frequency Coefficients of Foreman and Mobile & Calendar Sequences After 3-D Wavelet Transform

Temporal Subbands	Foreman		Mobile & Calendar	
	Spatial Subbands'	Temporal Subbands'	Spatial Subbands'	Temporal Subbands'
	Energy	Energy	Energy	Energy
<i>LLLL</i>	39779	6005	119298	5308
<i>LLLH</i>	1133	2172	2344	2056
<i>LLH<sub>0</sub></i>	319	199	390	62
<i>LLH<sub>1</sub></i>	757	515	1158	247
<i>LH<sub>0</sub></i>	53	36	56	20
<i>LH<sub>1</sub></i>	62	36	88	21
<i>LH<sub>2</sub></i>	76	32	123	26
<i>LH<sub>3</sub></i>	202	75	239	33

#### 4 3-D Significance Probability Balancing Tree

After weighting each subband, an appropriate tree structure is needed to better locate significant coefficients. Most previous asymmetrical structures pursue tree depth without considering the nodes' importance distribution on the same tree level. Table 2 shows average energy comparison between spatial and temporal high-frequency coefficients of the first 16 frames of "Foreman" and "Mobile & Calendar" sequences after 3-D wavelet transform. It can be seen that the average energy of different high-frequency subbands vary apparently, especially *LLLL* and *LLLH* subbands having the largest energy. The average amplitude of spatial high-frequency coefficients is larger than that of temporal high-frequency coefficients. This indicates that the probability of spatial high-frequency coefficients being significant is higher than that of temporal high-frequency coefficients. If both of them are placed on the same level, the latter has to be tested repeatedly before being significant so that the synchronization bits will be wasted. To address this issue, we present a novel 3-D tree structure named *significance probability balancing tree* in this section.

Our basic idea is to place those coefficients with similar probabilities of being significant on the same layer based on the amplitude correlation of spatio-temporal coefficients. To construct a significance probability balancing tree, one approach is to study the coefficients' distribution before each scan, and then to establish an adaptive tree structure. But the high computational demand will inhibit its practical use. Our proposed method processes the descendants of a parent node along its spatial and temporal orientation, respectively. The spatial descendants are arranged using spatial orientation tree of SPIHT, while the temporal descendants are organized from coarse to fine scales along temporal direction, selecting the spatial node with no offsprings as a root. Fig. 1 illustrates the parent-child relationship of the proposed tree. For the sake of clarity, only four temporal frames are shown with a 2-level temporal decomposition followed by a 1-level spatial decomposition.

Furthermore, adjacent wavelet coefficients in a subband tend to have identical importance [57]. We thus group adjacent  $2 \times 2$  coefficients into a block in

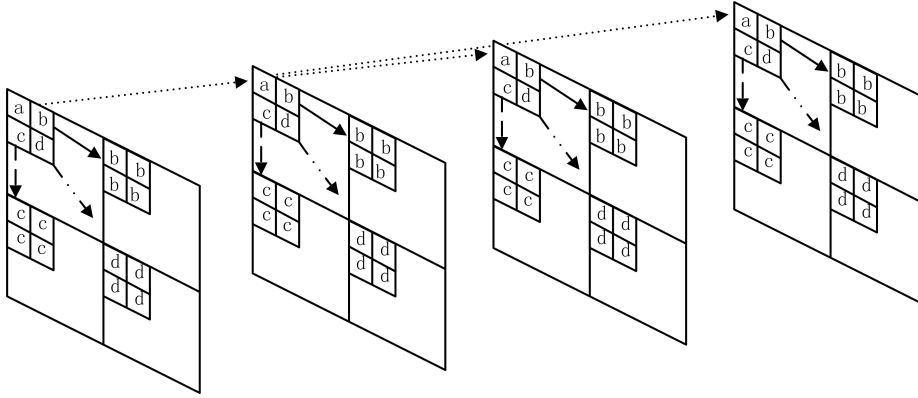


**Fig. 1** Parent-child relationship of the proposed 3-D significance probability balancing tree

the temporal high-frequency frames. Each block is treated as an offspring of the coefficient at the corresponding position in temporal low-frequency sub-band. The structure discussed above is named “*temporal-domain block tree*”. Only if a block contains the root(s) of nonzero subtree(s), the block will be divided into four coefficients, one of which is the root of a temporal-domain block tree. The other coefficients are separately the roots of three spatial orientation trees. Therefore, the proposed significance probability balancing tree is essentially a hybrid spatial orientation tree and temporal-domain block tree structure.

When using our proposed tree to organize 3-D wavelet coefficients, the synchronization information is coded block by block instead of coefficient by coefficient. Hence, this block-wise manner is able to reduce effectively the number of synchronization bits. In order to verify this point, we decompose the first 16 frames of “Foreman”, “Hall Monitor”, and “Mobile & Calendar” by 3-D wavelet transform and represent the resulting coefficients using our proposed tree and a typical asymmetric tree [54]. Subsequently, we calculate the ratio of degree-1 zerotree and degree-2 zerotree [61] under the above two tree structures, respectively. As depicted in Table 3, the proposed significance probability balancing tree can achieve higher zerotree ratio compared with the asymmetrical tree [54]. Fig. 2 presents part of quantized coefficients of temporal *LLLL* and *LLLH* frames of “Foreman”, where “2”, “1”, and “0” separately denote coded coefficients, significant coefficients, and insignificant coefficients. And the quantization step size is 256. Suppose that the coding of sign bits is ignored. Then the asymmetrical tree [54] needs a total of 40 bits namely “1101010100110001000010011100000000100010” to code significance map, while the significance probability balancing tree requires only 35 bits, i.e. “0110101010011 0001011100000000100 01”. For the other two sequences, a similar results can be obtained. Note that the above three test sequences belong to different classes of videos in MPEG-4 test library. “Foreman” has low spatial detail and medium amount of movement, while “Mobile & Calendar”



represents  $L(x, y)$ . Assuming  $T_i$  and  $T_0$  denotes quantization threshold of the  $i$ th scan and the initial threshold respectively, we detail the implementation of our proposed coding algorithm as below.

1. Parse the input video into a number of GOPs, and then apply 3-D wavelet transform to each GOP.
2. **Initialization.**

2.1 Calculate the initial threshold  $T_0$  for each GOP as follows

$$T_0 = \left\lfloor \log_2 \left( \max_{C_n \in C} |c_n| \right) \right\rfloor, \quad (2)$$

where  $C$  represents the 3-D wavelet coefficient set.

- 2.2 Set  $i = 0$  and  $LSP = \emptyset$ . Add the coefficients of lowpass subband in the temporally lowest-frequency frame, e.g. the upper-left “a”, “b”, “c” and “d” of the first frame as depicted in Fig. 1, to LIP and LIS, and set them in LIS as TYPE\_A entries.

### 3. Search for significant coefficients.

- 3.1 Compare each coefficient  $(x, y) \in LIP$  with  $T_i$ . If  $|(x, y)| \geq T_i$ , output “1” and its sign bit, and then move  $(x, y)$  to LSP. Otherwise, output “0”.
- 3.2 For each untreated  $(x, y) \in LIS$ , if it is a node of spatial orientation tree, e.g. “b”, “c”, and “d” of the first frame in Fig. 1, go to Step 3.3. Otherwise, if it is a node of temporal-domain block tree, e.g. “a” of the first frame in Fig. 1, go to Step 3.4.
- 3.3 Code  $(x, y)$  using SPIHT, go to Step 3.5.
- 3.4 If  $(x, y)$  is a TYPE\_B entry, go to Step 3.4.4. Else, if  $D(x, y)$  does not contain significant coefficients, output “0” and go to Step 3.5. Otherwise, output “1”.
  - 3.4.1 Check whether there are significant coefficients in  $(x, y)$ ’s temporal-domain child blocks, e.g. the upper-left “a”, “b”, “c”, and “d” of the second frame depicted in Fig. 1. If only insignificant coefficients are contained, output “0” and move  $(x, y)$  into the LIP. Go to Step 3.4.3.
  - 3.4.2 Otherwise, output “1” and test each node in every child block of  $(x, y)$ . For each significant coefficient, output “1” and sign bit, move it into LSP. For insignificant coefficient, output “0” and move it to LIP.
  - 3.4.3 If  $L(x, y) = \phi$ , remove  $(x, y)$  from LIS; Otherwise, move  $(x, y)$  to the end of the LIS as an entry of TYPE\_B and go to Step 3.5.
  - 3.4.4 If  $L(x, y)$  does not contain significant coefficients, output “0”. Otherwise, output “1”, and split current block into one root of temporal-domain block subtree and three roots of spatial directional tree. Move the four roots into LIS as entries of TYPE\_A and remove  $(x, y)$  from LIS.
- 3.5 If all  $(x, y) \in LIS$  have been coded, go to Step 4. Otherwise, go to Step 3.2.

#### 4. Refine the amplitudes of significant coefficients.

- 4.1 For each entry  $(x, y) \in \text{LSP}$ , if  $(x, y) \in [T_i, 1.5T_i)$ , output “0”. Otherwise, output “1”.
- 4.2 If target rate has been reached, return. Otherwise, Set  $i = i + 1$ ,  $t_i = T_{i-1}/2$ .
- 4.3 If  $T_i = 0$ , return. Else, go to Step 3.

## 6 Experimental Results and Analysis

Extensive experiments were conducted on seven color video sequences including the first 128 frames of “Foreman”, “Hall Monitor”, “Mobile & Calendar”, “Coastguard”, “Mother & Daughter”, “Miss America”, and “Bus” in CIF@30Hz format. All experiments were performed on VidWav platform [27]. The 3-D wavelet transform was decomposed in “t+2D” manner with 4-level 5/3 motion-compensated temporal filtering and 3-level 2-D 9/7 wavelet. Motion estimation were carried out with quarter-pixel accuracy. For each color video sequence, its Y, U, and V components were sequentially encoded.

To verify the effectiveness of our algorithm, we compare it against two representative methods, i.e. the asymmetric 3-D orientation tree [54] and temporal-spatial orientation tree [56], in terms of peak signal-to-noise ratio (PSNR). Note that, the PSNR statistics of [54] were obtained on VidWav platform, while the results of temporal-spatial orientation tree were extracted from [56] which only presented the PSNRs for “Foreman”, “Miss America”, and “Mobile & Calendar”. Table 4 shows the PSNR comparison result among the above three coding algorithms at 128Kbps-1500Kbps for “Miss America”, “Foreman”, and “Mobile & Calendar”. Table 5-Table 8 list the comparison results between the asymmetric 3-D orientation tree and our proposed algorithm for “Hall Monitor”, “Mother & Daughter”, “Coastguard”, and “Bus” at 128Kbps-1500Kbps.

As can be seen from Table 4-Table 8, asymmetric 3-D orientation tree outperforms temporal-spatial orientation tree for those sequences with low amount of movement, such as Miss America and Foreman, while the latter gains superior efficiency to the former for sequences with high spatial detail and medium amount of movement, such as Mobile & Calendar. This indicates that these two tree structures have distinct merits and their performances always depend on the characteristics of video sequences. Since our algorithm takes into consideration the coefficients’ significance probability distribution on the same tree level, it is less sensitive to video characteristics and achieves the highest PSNR for all test sequences. For Y component, the average PSNR of proposed algorithm is separately 1.24dB and 0.38dB higher than those of [54] and [56]. While for U and V components, our algorithm gains 2.54dB and 2.57dB higher PSNR compared with [54], and 2.92dB and 2.39dB higher PSNR than [56]. It is worth mentioning that for the Y component of “Mobile & Calendar”, the PSNR achieved by our algorithm is lower than that of [56] as shown in Table 4. According to the experimental results presented in [56], the PSNR

**Table 4** PSNR Comparison Among Three Test Algorithms at Different Bitrates

Test Sequence	Bitrate (Kbps)	PSNR (dB)								
		Asymmetric Tree			Temporal-spatial Tree			Proposed Tree		
		Y	U	V	Y	U	V	Y	U	V
<b>Miss America</b>	128	39.99	38.35	40.41	—	—	—	40.88	39.10	41.99
	256	40.57	38.73	41.01	—	—	—	42.38	39.92	43.35
	384	41.91	39.84	42.14	—	—	—	43.05	40.45	43.95
	500	42.34	40.23	42.54	41.76	40.64	42.27	43.38	40.83	44.17
	768	42.78	40.68	43.11	—	—	—	44.04	41.84	44.68
	1000	42.88	40.84	43.23	43.23	40.69	43.46	44.36	42.51	45.00
	1500	43.96	42.32	44.42	43.99	40.69	43.46	44.84	43.82	45.52
<b>Foreman</b>	128	29.04	35.45	35.41	—	—	—	29.80	37.53	37.39
	256	32.30	37.87	38.38	—	—	—	33.32	39.79	40.43
	384	33.79	38.70	39.86	—	—	—	35.07	40.90	42.10
	500	35.04	39.52	40.97	34.84	37.63	39.42	36.18	41.71	43.08
	768	36.37	40.49	42.20	—	—	—	37.81	43.12	44.51
	1000	37.54	41.26	43.26	37.76	39.63	41.76	38.96	44.01	45.37
	1500	38.99	42.72	44.71	39.40	40.50	42.62	40.51	45.42	46.66
<b>Mobile &amp; Calendar</b>	128	20.38	25.99	24.75	—	—	—	20.76	27.87	26.38
	256	23.15	28.28	27.19	—	—	—	23.99	30.31	29.06
	384	24.63	29.21	28.45	—	—	—	25.71	31.84	30.67
	500	25.05	29.52	28.83	27.38	30.92	30.97	26.97	33.54	32.44
	768	27.55	31.28	30.92	—	—	—	28.57	35.19	34.35
	1000	28.56	32.28	32.07	31.26	34.38	34.55	29.82	36.82	36.01
	1500	30.00	33.70	33.36	33.49	35.77	35.99	31.49	38.47	37.76

improvement of [56] is separately 0.18dB, 0.34dB, and 0.41dB at 500Kbps, 1000Kbps, and 1500Kbps compared with [54]. Nevertheless, our algorithm obtains 1.92dB, 1.26dB, and 1.49dB higher PSNR than those of [54] at the above bitrates, respectively. In this sense, our algorithm still outperforms [56] regarding the Y component of “Mobile & Calendar”.

In addition, the ratio of zerotrees is increased after the wavelet coefficients are weighted, as illustrated in Table 3. Thus, the number of isolated zeroes is effectively reduced, which always involve many comparisons and input/output operations in conventional zerotree coding algorithms. Further, since the proposed temporal-domain block tree operates on units of size  $2 \times 2$  pixels, the number of entries in LIP and LIS is less than that of [54] and [56]. On one hand, the energy-based weight and temporal-domain block tree are capable of improving the efficiency of synchronization information. On the other hand, they help to lower the computational complexity of video coding algorithm. Of course, with the increase of target bitrate, the temporal-domain block trees need to be recursively split, the computational complexity will gradually close to that of [54, 56].

**Table 5** PSNR Comparison Between Asymmetric 3-D Orientation Tree Algorithm and Our Algorithm at Different Bitrates for “Hall Monitor” sequence

Bitrate (Kbps)	Asymmetric 3-D Tree			Proposed Algorithm		
	Y	U	V	Y	U	V
128	31.01	36.47	38.88	31.96	37.68	40.21
256	34.64	37.57	39.72	36.46	39.28	41.46
384	36.71	38.42	40.57	38.10	39.89	42.14
500	37.32	38.72	40.82	38.96	40.32	42.48
768	38.54	39.77	41.57	40.14	41.16	43.03
1000	39.22	40.69	42.08	40.74	41.71	43.43
1500	39.68	41.43	42.52	41.70	42.66	44.16

**Table 6** PSNR Comparison Between Asymmetric 3-D Orientation Tree Algorithm and Our Algorithm at Different Bitrates for “Mother & Daughter” sequence

Bitrate (Kbps)	Asymmetric 3-D Tree			Proposed Algorithm		
	Y	U	V	Y	U	V
128	35.20	40.52	41.18	36.25	42.90	43.40
256	38.57	42.40	43.54	39.55	44.85	45.73
384	40.27	43.56	44.71	41.19	45.97	46.67
500	41.36	44.45	45.48	42.36	46.64	47.42
768	42.48	45.50	46.20	43.83	47.56	48.42
1000	43.59	46.26	47.00	44.70	48.10	48.98
1500	44.56	47.14	47.91	45.62	48.64	49.52

**Table 7** PSNR Comparison Between Asymmetric 3-D Orientation Tree Algorithm and Our Algorithm at Different Bitrates for “Coastguard” sequence

Bitrate (Kbps)	Asymmetric 3-D Tree			Proposed Algorithm		
	Y	U	V	Y	U	V
128	24.96	37.63	36.24	25.58	40.40	41.66
256	26.35	38.40	37.51	27.61	41.63	43.32
384	27.94	40.06	41.06	28.89	42.45	44.14
500	28.67	40.29	41.16	29.80	42.99	44.54
768	29.88	40.89	42.09	31.29	43.64	45.18
1000	31.32	41.38	43.14	32.52	44.22	45.73
1500	33.10	42.10	43.66	34.30	45.02	46.48

## 7 Conclusions

In this study, by analyzing the contribution of each biorthogonal wavelet basis in terms of its reconstructed energy, we proposed to weight each subband by the energy of its corresponding basis before encoding. According to the distribution of weighted coefficients, we put forward a concept of 3-D significance

**Table 8** PSNR Comparison Between Asymmetric 3-D Orientation Tree Algorithm and Our Algorithm at Different Bitrates for “Bus” sequence

Bitrate (Kbps)	Asymmetric 3-D Tree			Proposed Algorithm		
	Y	U	V	Y	U	V
128	21.04	31.49	29.87	21.43	34.56	35.67
256	24.42	34.40	34.95	25.14	36.49	37.79
384	25.84	34.99	35.71	27.01	37.36	38.87
500	27.28	35.94	37.13	28.09	37.82	39.45
768	29.13	36.62	38.03	30.37	39.16	40.92
1000	30.10	37.30	38.76	31.48	39.69	41.44
1500	32.41	38.30	39.99	34.03	41.37	43.01

probability balancing tree structure and implement it using hybrid spatial orientation tree and temporal-domain block tree. Consequently, a novel 3-D wavelet video coding algorithm is presented based on energy-weighted significance probability balancing tree. We verify its effectiveness through extensive experiments. We believe that our study will be certainly useful in future researches and developments of wavelet-based scalable video coding.

**Acknowledgements** This work is supported by the National Natural Science Foundation of China (NSFC) under Grant nos. 61402214, 41671439, and 61702246, and the Open Foundation of State Key Laboratory for Novel Software Technology of Nanjing University under Grant no. KFKT2018B07, and the Dalian Foundation for Youth Science and Technology Star (2015R069).

## References

1. SVC requirements specified by MPEG, JVT-N026, Tech. rep., ISO/IEC JTC1/SC29/WG11, Hong Kong (2005).
2. Y. Liu, J. Y. B. Lee, Post-streaming rate analysis a new approach to mobile video streaming with predictable performance, *IEEE Transactions on Mobile Computing* 16 (12) (2017) 3488–3501.
3. R. Shah, P. J. Narayanan, Interactive video manipulation using object trajectories and scene backgrounds, *IEEE Transactions on Circuits and Systems for Video Technology* 23 (9) (2013) 1565–1576.
4. L. Wu, Y. Wang, J. Gao, X. Li, Deep adaptive feature embedding with local sample distributions for person re-identification, *Pattern Recognition* 73 (1) (2018) 275–288.
5. L. Wu, Y. Wang, X. Li, J. Gao, What-and-where to match: Deep spatially multiplicative integration networks for person re-identification, *Pattern Recognition* 76 (1) (2018) 727–738.
6. L. Wu, Y. Wang, Z. Ge, Q. Hu, X. Li, Structured deep hashing with convolutional neural networks for fast person re-identification, *Computer Vision and Image Understanding* 167 (1) (2018) 63–73.
7. Y. Wang, X. Lin, L. Wu, W. Zhang, Effective multi-query expansions: Collaborative deep networks for robust landmark retrieval, *IEEE Transactions on Image Processing* 26 (3) (2017) 1393–1404.
8. Y. Wang, L. Wu, Beyond low-rank representations: Orthogonal clustering basis reconstruction with optimized graph structure for multi-view spectral clustering, *Neural Networks* 103 (1) (2018) 1–8.

9. L. Wu, Y. Wang, X. Li, J. Gao, Deep attention-based spatially recursive networks for fine-grained visual recognition, *IEEE Transactions on Cybernetics* 99 (PP). doi:10.1109/TCYB.2018.2813971.
10. Y. Wang, X. Lin, L. Wu, W. Zhang, Q. Zhang, X. Huang, Robust subspace clustering for multi-view data by exploiting correlation consensus, *IEEE Transactions on Image Processing* 24 (11) (2015) 3939–3949.
11. Y. Wang, W. Zhang, L. Wu, X. Lin, X. Zhao, Unsupervised metric fusion over multiview data by graph random walk-based cross-view diffusion, *IEEE Transactions on Neural Networks and Learning Systems* 28 (1) (2017) 57–70.
12. Y. Wang, W. Zhang, L. Wu, X. Lin, M. Fang, S. Pan, Iterative views agreement: An iterative low-rank based structured optimization method to multi-view spectral clustering, in: *Proc. International Joint Conference on Artificial Intelligence*, Vol. 1, New York, USA, 2016, pp. 2153–2159.
13. Y. Wang, L. Wu, X. Lin, J. Gao, Multiview spectral clustering via structured low-rank matrix factorization, *IEEE Transactions on Neural Networks and Learning Systems* 99 (PP). doi:10.1109/TNNLS.2017.2777489.
14. H. Schwarz, D. Marpe, T. Wiegand, Overview of the scalable video coding extension of the H.264/AVC standard, *IEEE Transactions on Circuits and Systems for Video Technology* 17 (9) (2007) 1103–1120.
15. T. Wiegand, G. J. Sullivan, J. Reichel, H. Schwarz, H. Wien, Joint draft 11 of SVC amendment, Doc. JVT-X201, Tech. rep., Geneva, Switzerland (2007).
16. U.-K. Park, H. Choi, J. W. Kang, J.-G. Kim, Scalable video coding with large block for UHD video, *IEEE Transactions on Consumer Electronics* 28 (3) (2012) 932–940.
17. A. Bjelopera, S. Grgic, Scalable video coding extension of H.264/AVC, in: *Proc. International Symposium ELMAR*, Vol. 1, Zadar, Croatia, 2012, pp. 7–12.
18. ISO/IEC JTC 1/SC 29/WG 11 and ITU-T SG 16 WP 3, Joint call for proposals on scalable video coding extensions of high efficiency video coding (HEVC), Tech. Rep. N12957, Stockholm, Sweden (2012).
19. Z. Shi, X. Sun, F. Wu, Spatially scalable video coding for HEVC, *IEEE Transactions on Circuits and Systems for Video Technology* 22 (12) (2012) 1813–1826.
20. G. Wu, W. Ding, Y. Shi, B. Yin, Adaptive weighted prediction for scalable video coding based on HEVC, in: *Proc. Pacific Rim Conference on Multimedia (PCM)*, Vol. 1, London, 2013, pp. 110–121.
21. S. Lasserre, F. L. Leanne, J. Taquet, E. Nassor, Low-complexity intra coding for scalable extension of HEVC based on content statistics, *IEEE Transactions on Circuits and Systems for Video Technology* 24 (2014) (to be published).
22. D. Marpe, H. L. Cycon, Very low bit-rate video coding using wavelet-based techniques, *IEEE Transactions on Circuits and Systems for Video Technology* 9 (1) (1999) 85–94.
23. E. Khan, M. Ghanbari, An efficient and scalable low bit-rate video coding with virtual SPIHT, *Signal Processing: Image Communication* 19 (3) (2004) 267–283.
24. M. S. Zhong, M. Ghanbari, Motion compensation based on wavelet coefficient blocks, *Acta Automatica Sinica* 30 (1) (2004) 64–69.
25. B. Kim, Z. Xiong, W. A. Pearlman, Low bit rate, scalable video coding with 3-D set partitioning in hierarchical trees (3-D SPIHT), *IEEE Transactions on Circuits and Systems for Video Technology* 10 (12) (2000) 1374–1387.
26. P. S. Chen, J. W. Woods, Bidirectional MC-EZBC with lifting implementation, *IEEE Transactions on Circuits and Systems for Video Technology* 14 (10) (2004) 1183–1194.
27. ISO/IEC JTC1/SC29/WG11, Wavelet codec reference document and software manual, Tech. Rep. ISO/MPEG Video, Tech. Rep. N7334 (Jul. 2005).
28. M. F. López, V. G. Ruiz, I. García, Efficiency of closed and open-loop scalable wavelet based video coding, *Advanced Concepts for Intelligent Vision Systems*, Lecture Notes in Computer Science 4678 (10) (2007) 800–809.
29. W. Ding, J. Hu, L. Zhang, Optimal 3D-SPIHT video coding method by reducing redundancy between trees, *Journal of Computer-Aided Design & Computer Graphics* 17 (3) (2005) 563–569.
30. C. C. Cheng, G. J. Peng, W. L. Hwang, Subband weighting with pixel connectivity for 3-D wavelet coding, *IEEE Transactions on Image Processing* 18 (1) (2009) 52–62.
31. P. Chen, J. W. Woods, Improved MC-EZBC with quarter-pixel motion vectors, Tech. rep., ISO/IEC JTC 1/SC 29/WG 11, Fairfax, VA.

32. R. Xiong, J. Xu, F. Wu, S. Li, Barbell-lifting based 3-D wavelet coding scheme, *IEEE Transactions on Circuits and Systems for Video Technology* 17 (9) (2007) 1256–1269.
33. S. Fang, Y. Zhong, 3D subband codec with full scalability, *Mini-Micro Systems* 26 (7) (2005) 1260–1263.
34. T. J. H. Wang, J. Zhang, Z. Jiang, Research on the scalability of 3D wavelet video coding, *Mini-Micro Systems* 26 (2) (2005) 285–288.
35. Z. Chang, L. Zhuo, L. Shen, An improved motion-compensated three dimension wavelet video coding method, *Journal of Circuits and Systems* 11 (1) (2006) 113–117, 121.
36. ISO/IEC JTC 1/SC 29/WG 11, Wavelet video coding - an overview, Doc. W7824, Bangkok, Thailand (2006).
37. ISO/IEC JTC 1/SC 29/WG 11, Status report - version 1 on wavelet video coding exploration, Doc. N7822, Bangkok, Thailand (2006).
38. X. Lu, G. R. Martin, Performance comparison of the SVC, WSVC, and Motion JPEG2000 advanced scalable video coding schemes, in: *Proc. IET, Intelligent Signal Processing*, Vol. 1, London, 2013, pp. 1–6.
39. D. Taubman, High performance scalable image compression with EBCOT, *IEEE Transactions on Image Processing* 9 (7) (2000) 1158–1170.
40. J. Shapiro, Embedded image coding using zerotree of wavelet coefficients, *IEEE Transactions on Signal Processing* 41 (12) (1993) 3445–3462.
41. A. Said, W. A. Pearlman, A new, fast, and efficient image codec based on set partitioning in hierarchical trees, *IEEE Transactions on Circuits and Systems for Video Technology* 6 (3) (1996) 243–250.
42. B. Chai, J. Vass, X. Zhuang, Significance link connected component analysis for wavelet image coding, *IEEE Transactions on Image Processing* 8 (6) (1999) 774–784.
43. W. A. Pearlman, A. Islam, N. Nagaraj, A. Said, Efficient low-complexity image coding with set-partitioning embedded block coder, *IEEE Transactions on Circuits and Systems for Video Technology* 14 (11) (2004) 1219–1235.
44. S. T. Hsiang, J. W. Woods, Embedded image coding using zeroblocks of subband/wavelet coefficient and context modeling, in: *Proc. IEEE International Symposium on Circuit and Systems (ISCAS'00)*, Vol. 3, Geneva, Switzerland, 2000, pp. 662–665.
45. A. A. Moinuddin, E. K. E. M. Ghanbari, The impact of tree structures on the performance of zerotree-based wavelet video codecs, *Signal Processing: Image Communication* 25 (3) (2010) 179–195.
46. J. E. Fowler, B. Pesquet-Popescu, An overview on wavelets in source coding, communications, and networks, *EURASIP Journal on Image and Video Processing* 2007 (1) (2007) 1–27.
47. P. Campisi, M. Gentile, A. Neri, Three-dimensional wavelet-based approach for a scalable video conference system, in: *Proc. IEEE International Conference on Image Processing (ICIP'99)*, Vol. 3, Kobe, Japan, 1999, pp. 802–806.
48. J. Vass, B. Chai, X. Zhuang, 3-D SLCCA—a highly scalable very low bit-rate software-only wavelet video codec, in: *Proc. IEEE Second Workshop Multimedia Signal Processing*, Vol. 3, Redondo Beach, CA, 1998, pp. 474–479.
49. B. J. Kim, W. A. Pearlman, An embedded wavelet video coder using three-dimensional set partitioning in hierarchical trees (SPIHT), in: *Proc. Data Compression Conference*, Vol. 1, Snowbird, USA, 1997, pp. 251–260.
50. J. Xu, Z. Xiong, S. Li, Y.-Q. Zhang, Three-dimensional embedded subband coding with optimal truncation (3-D ESCOT), *Applied Computational Harmonic Analysis* 10 (3) (2001) 290–315.
51. Y. Chen, W. A. Pearlman, Three-dimensional subband coding of video using the zerotree method, in: *Proc. SPIE Visual Communications and Image Processing*, Vol. 2727, Snowbird, USA, 1996, pp. 1302–1312.
52. H. Khalil, F. A. F. S. I. Shaheen, Lowering frame-buffering requirements of 3-D wavelet transform coding of interactive video, in: *Proc. IEEE International Conference on Image Processing (ICIP'99)*, Vol. 3, Kobe, Japan, 1999, pp. 852–856.
53. G. Minami, Z. Xiong, A. Wang, P. A. Chou, S. Mehrotra, 3-D wavelet coding of video with arbitrary regions of support, *IEEE Transactions on Circuits and Systems for Video Technology* 11 (9) (2001) 1063–1068.

54. C. He, J. Dong, Y. Zheng, Z. Gao, Optimal 3-D coefficient tree structure for 3-D wavelet video coding, *IEEE Transactions on Circuits and Systems for Video Technology* 13 (10) (2003) 961–972.
55. E. Khan, M. Ghanbari, Very low bit rate video coding using virtual spiht, *Electronic Letters* 37 (1) (2001) 40–41.
56. L. Zhang, D. Wang, A. Vincent, Decoupled 3-D zerotree structure for wavelet-based video coding, *IEEE Transactions on Broadcasting* 54 (3) (2008) 430–436.
57. C.-M. Song, X.-H. Wang, F. Zhang, Visually lossless accuracy of motion vector in over-complete wavelet-based scalable video coding, *Journal of Computers* 4 (9) (2009) 821–828.
58. A. A. Moinuddin, E. Khan, M. Ghanbari, Efficient and embedded 3-D wavelet video coding, in: *Proc. TENCON 2008, Vol. 1, Hyderabad, 2008*, pp. 1–4.
59. B. Usevitch, Optimal bit allocation for biorthogonal wavelet coding, in: *Proc. Data Compression Conference, Vol. 1, Snowbird, USA, 1996*, pp. 387–395.
60. B. E. Usevitch, A tutorial on modern lossy wavelet image compression: foundations of JPEG 2000, *IEEE Signal Processing Magazine* 18 (5) (2001) 22–35.
61. Y. Cho, W. A. Pearlman, Quantifying the coding performance of zerotrees of wavelet coefficients: degree-k zerotree, *IEEE Transactions on Signal Processing* 55 (6) (2007) 2425–2431.